Mechanisms and Precipitation Rate of Rhodochrosite at 25°C as Affected by P_{CO2} and Organic Ligands

I. Lebron* and D. L. Suarez

ABSTRACT

Rhodochrosite is the main Mn mineral phase in neutral to alkaline anoxic environments and is likely the initial precipitation phase when Mn^{2+} is added to irrigation water. Solutions supersaturated with respect to rhodochrosite that was detected in various natural environments suggest that equilibrium assumptions may not be satisfactory and kinetic processes may be dominant. This study was conducted to evaluate the precipitation mechanisms of rhodochrosite in natural environments where DOC is present and there are variations in partial pressure of CO_2 (P_{CO2}). Precipitation rates were measured in supersaturated solutions of rhodochrosite in the presence of seeds of the mineral and P_{CO2} 0.035 kPa, 5 kPa, and 10 kPa and in a concentration range of DOC of 0.02 to 3.2 m*M* of Suwannee River fulvic acid. Precipitation rates were measured in the absence and presence of 1 m*M* leonardite humic acid. Precipitation rates increased when the P_{CO2} increased and decreased when the concentration of the fulvic acid increased at constant levels of supersaturation. However, higher concentrations of DOC were needed to produce the same reduction in precipitation rates when P_{CO2} was increased. The most likely causes of the increase in the precipitation rate when P_{CO2} increases are an increase in the negative surface charge and an increase in the activity of $MnHCO_3^+$. No significant change in the precipitation rate of rhodochrosite was measured when the leonardite humic acid was added to the reaction vessels. The lack of inhibition of leonardite humic acid on rhodochrosite precipitation is explained by its molecular configuration in solution.

MANGANESE IS THE SECOND MOST ABUNDANT HEAVY METAL in the crust after Fe, to which it has many geochemical similarities (Crerar et al., 1980). Manganese is also an essential micronutrient for plants, and its cycle in oxic–anoxic boundaries is associated with several soil biogeochemical processes, such as microbial respiration, scavenging and transport of heavy metals, and oxidation of humic substances (Balistrieri and Murray, 1982; Friedl et al., 1997).

The oxidation state of Mn in natural environments varies from +2 to +4; however, due to solubility considerations only Mn^{2+}-containing species are expected in the soil solution across the range of pE and pH of most soils (Norvell, 1988). Manganese (II) and its complexes constitute the principal transport species (Wolfram and Krupp, 1996) and are the predominant forms taken up by plant roots (Marschner, 1988). In arid-zone regions, where calcareous soils with high pH and high content of calcite ($CaCO_3$) are abundant, low Mn availability may be a limiting factor for plant growth. Addition of Mn^{2+} directly to the irrigation water has been proposed and is practiced as a component of fertigation. Formation of rhodochrosite ($MnCO_3$) is typically associated with $CaCO_3$ as a (Mn, Ca)CO_3 solid solution, as shown in numerous studies Pederson and Price, 1982; Jackobsen and Postma, 1989; Wartel et al., 1990; Okita, 1992, Boyle, 1983, Friedl et al., 1997). Under anoxic conditions and independent of the specific mineral phase, Mn chemistry in soils is constrained by the carbonate solution chemistry.

Many efforts have been devoted to the study of the carbonate chemistry in the last 50 years. This attention is justified if we consider that in neutral to alkaline environments, carbonates control all the pH-dependent processes, such as the surface mineral–water interactions, transport, and bioavailability of micronutrients to plants. Predicting the rate of carbonate precipitation is essential in any attempt to model solute transport in soils and to prevent undesired precipitation in irrigation systems.

The concentration of Mn and CO_3 in sedimentary environments frequently yields saturation index (Ω) values >1 for rhodochrosite ($\Omega = IAP/K_{sp}$, where IAP is the ionic activity product, and K_{sp} is the solubility product of pure mineral phase at 25°C). The results of Jackobsen and Postma (1989) showed slow rhodochrosite precipitation in porewaters from the Baltic Deeps, indicating that the solid solutions of (Mn, Ca)CO_3 are metastable and kinetically regulated (Sternbeck, 1997). These studies suggest that equilibrium assumptions may not be satisfactory for predicting Mn^{2+} in solution, and that kinetics processes may be dominant.

The only reported experiment on the kinetics of rhodochrosite precipitation is that performed by Sternbeck (1997). Sternbeck studied the crystal growth of rhodochrosite at 25°C and applied the surface speciation model of van Cappellen et al. (1993) to describe the process. Nevertheless, it has been shown for the calcite system that small amounts of DOC inhibit the precipitation rate of carbonates by blocking crystal growth (Kitano and Hood, 1965; Reddy, 1977; Reynolds, 1978; Reddy and Wang, 1980; Inskeep and Bloom, 1986; Dove and Hochella, 1993; Gratz and Hillner, 1993; Katz et al. 1993, Paquette et al., 1996; Lebron and Suarez, 1996). Inhibition occurs as a result of adsorption of DOC molecules onto the surface of the carbonate crystals (Inskeep and Bloom, 1986; Lebron and Suarez, 1996). Fulvic acids have been found to be more efficient in inhibiting calcite precipitation than the DOC obtained from a soil extract. However, fulvic and humic acids from a soil extract are more efficient than small organic molecules like citric, gallic, syringic, adipic, and azealic acids in the reduction of hydroxyapatite precipitation (Inskeep and Silver-

U.S. Salinity Lab., USDA-ARS, 450 W. Big Springs Rd., Riverside, CA 92507. Contribution from the U.S. Salinity Lab. Received 27 Apr. 1998. *Corresponding author (lebron@ucracl.ucr.edu).

Published in Soil Sci. Soc. Am. J. 63:561–568 (1999).

Abbreviations: DIW, deionized water; DOC, dissolved organic carbon; IHSS, International Humic Substances Society; pH_{ZPC}, pH of zero point of charge.

tooth, 1988). The efficiency of organic molecules in inhibiting mineral precipitation is attributed to the nature and number of functional groups (phenolic, carboxylate, etc).

The blocking of calcite crystal growth by organic matter has been found by Lebron and Suarez (1996) to occur at levels of DOC comparable to those found in natural environments. Thus, heterogeneous nucleation is the dominant mechanism for calcite precipitation in soils, sediments, and most surface and ground water. In addition, knowledge of the carbonate precipitation rates at different P_{CO2} levels is important, since in both the soil root zone and in sediments P_{CO2} is 10 to 500 times higher than atmospheric. The P_{CO2} and suspension composition determine the chemical speciation of Mn^{2+} in solution and at the mineral surface. In turn, dissolution and precipitation kinetics of carbonate minerals depend on the chemical speciation and electrical charge of the mineral–aqueous solution interface.

The objectives of this study are: (i) to evaluate the applicability of rhodochrosite equilibrium data in order to predict aqueous Mn^{2+} concentrations in natural systems, (ii) to study the precipitation mechanism of rhodochrosite as related to soils and other natural environments, (iii) to measure the precipitation rate of rhodochrosite as affected by P_{CO2}, fulvic acid, and leonardite humic acid reference materials, and (iv) to formulate a rate model to predict the kinetics of precipitation of rhodochrosite at different supersaturation levels and different P_{CO2} and DOC concentrations.

MATERIALS AND METHODS

Suwannee River fulvic acid and leonardite humic acid reference (International Humic Substances Society [IHSS]) were used to study the influence of organic ligands on the mechanisms and rate of precipitation of rhodochrosite. The fulvic acid was dissolved in deionized water (DIW); leonardite humic acid was also dissolved in DIW by addition of NaOH and adjusted to pH 7.5. Both solutions were filtered through 0.2-μm Whatman[1] filters, analyzed for DOC with a Dohrmann Carbon Analyzer (Dohrmann, Santa Clara, CA 95050), and stored at 4°C until used.

We prepared supersaturated solutions of rhodochrosite (Analyzed Reagent Grade, Aldrich Chemical, St. Louis, MO) as follows: an excess of rhodochrosite was placed in a volumetric flask and dissolved in DIW for 24 h under a P_{CO2} of 100 kPa. This solution was then bubbled with a gas that has a P_{CO2} lower than 100 kPa, which yielded a supersaturated solution; from this supersaturated solution a range of Ω values was generated by dilution with DIW.

For the crystal growth experiments, rhodochrosite seeds were freshly prepared in the laboratory to avoid any oxidation on the crystal surfaces. A mixture of $NaHCO_3$ and $MnCl_2$ solutions were used to precipitate $MnCO_3$ while the solution was bubbled with N_2. The precipitate was filtered, washed, and dried in a N_2 atmosphere in the absence of light. The precipitate was characterized using X-ray diffraction, scanning electron microscopy, and microprobe analysis (Princeton Gamma-Tech, Princeton, NJ). The 2- to 20-μm fraction was collected by sedimentation after suspending the particles in DIW. Surface area was measured by single-point BET N_2 adsorption with a Quantachrome Quantasorb Jr. surface area analyzer (Quantacrome Corp., Syosset, NY). The specific surface area of the synthetic rhodochrosite crystals was 3.3 ± 0.01 $m^2\ g^{-1}$.

Precipitation experiments were performed using 250-mL flasks; the walls of the flasks were covered with aluminum foil to avoid Mn oxidation, and each was connected to a N_2–CO_2 gas source by a plastic capillary inserted into the flask's stopper. The gas was presaturated with water to avoid evaporation in the samples. The N_2 and CO_2 gas composition in the flasks was maintained using individual Edwards model 825 mass flow controllers and was monitored by an Edwards model 1605 multichannel flow controller (Edwards High Vacuum International, Wilmington, MA).

Samples from the supernatant were taken at intervals and filtered through prerinsed 0.1-μm filters. A portion of the filtered sample was diluted 5-fold to avoid further precipitation and analyzed for Mn and alkalinity. Manganese was determined by inductively coupled plasma emission spectroscopy, and alkalinity was measured by titration with $KH(IO_3)_2$ (National Bureau of Standards primary acid standard). The titration was made as described in Suarez et al. (1992). The other portion of the filtered sample was acidified with HNO_3, bubbled for 5 min with O_2, and analyzed for DOC with a Dohrmann Carbon Analyzer (Dohrmann, Santa Clara, CA). The pH of the suspensions was measured at the time of sampling with a Fisher Accumet 520 pH meter (Fisher Scientific Co., Pittsburgh, PA) and a Thomas 4094 combination pH electrode (Thomas Scientific, Swedesboro, NJ) calibrated with buffers pH 4.00 and 6.86 to within 0.01 pH units at 25°C.

The saturation indices, Ω, for $MnCO_3$ were calculated for every sampling from pH and the activities of the free Mn^{2+} and CO_3^{2-} in solution using the speciation program GEOCHEM-PC (Parker et al., 1994). The constant used to quantify the complexation of the fulvic acid with Mn was pK = 2.7, which corresponds to one of the two fulvic acids listed in GEOCHEM ($FUL2^-$). The choice of $FUL2^-$ was based on the similarities of the elemental chemical composition and the infrared spectra of this fulvic acid with Suwannee fulvic acid. Chemical elemental analysis and infrared spectra of the $FUL2^-$ was performed by Sposito et al. (1976) and FTIR of Suwannee fulvic acid reference by Lebron and Suarez (1996). The chemical composition of Suwannee fulvic acid was provided by the IHSS.

The precipitation rate of rhodochrosite in a given time interval was calculated by subtracting the Mn^{2+} concentration at $t = 0$ from the Mn^{2+} concentration at $t = 1$ and dividing by the number of seconds between the two sampling times. Similar calculations were also made using the changes in the HCO_3^- concentration. The precipitation rate of rhodochrosite calculated from the Mn^{2+} data and from the HCO_3^- data were in good agreement as expected (within 1%). All flasks were covered with aluminum foil and shaken on a reciprocating shaker table at 90 cpm during the experiment. The experiments were carried out in a constant temperature room at 25 ± 0.5°C. A flask containing 1 m*M* of $NaHCO_3$ was used as a control to check for possible evaporation. All samples were duplicated and standard deviations calculated.

Crystal Growth as Affected by Dissolved Organic Carbon and P_{CO2}

From preliminary experiments, we determined that solutions with $\Omega \leq 3$ did not precipitate in the absence of rhodochrosite crystals. We assume that the precipitation by heterogeneous nucleation is negligible under these conditions and

[1] Trade names are provided for the benefit of the reader and do not imply any endorsement by the USDA.

that crystal growth is the dominant mechanism of precipitation. The precipitation rate of rhodochrosite was measured at $\Omega = 3$ in the presence of 10 $m^2 L^{-1}$ of rhodochrosite crystal seeds and in the range of 0 to 0.8 m*M* DOC obtained from Suwannee fulvic acid. Samples were taken at time 0 and 1 h, and the test was terminated when precipitation was observed in the flask. The rationale for small time intervals is to avoid large changes in Ω. Erlenmeyer flasks with no precipitation during the first hour were sampled periodically until precipitation occurred, up to a total of 3 d. The precipitation rate was measured at 0.035, 5, and 10 kPa P_{CO_2}, with all samples run in duplicate. The Mn activity was calculated with GEOCHEM-PC, taking into account Mn–fulvic complexation.

Heterogeneous Nucleation as Affected by Dissolved Organic Carbon and P_{CO_2}

The precipitation rate of rhodochrosite was measured at constant Ω ($\Omega = 25$) in the DOC concentration range of 0 to 4 m*M* and in the presence of 2 $m^2 L^{-1}$ of rhodochrosite crystals. The crystals had previously been coated with an amount of DOC necessary to inhibit precipitation by crystal growth; the amount of DOC used is specified below in the discussion section. Precipitation was measured in duplicate at 0.035, 5, and 10 kPa P_{CO_2}. The Ω values were calculated using Mn activities corrected for Mn–fulvic acid complexation.

Kinetics of Rhodochrosite Precipitation as Affected by Dissolved Organic Carbon and P_{CO_2}

Precipitation rate of rhodochrosite was measured in the presence of 2 $m^2 L^{-1}$ of rhodochrosite crystals and with Suwannee fulvic acid concentrations of 0.02 to 1.4 m*M* for P_{CO_2} = 0.035 kPa, 0.02 to 2.10 m*M* DOC for 5 kPa, and 0.02 to 3.20 m*M* DOC for 10 kPa. The precipitation rate of rhodochrosite was also measured in solutions with (i) no addition of leonardite and (ii) 1 m*M* DOC obtained from leonardite humic acid reference. Supersaturated solutions were allowed to react for a total of 24 h. Solution samples were removed at $t = 0$, 0.5, 1, 2, and 24 h.

RESULTS AND DISCUSSION

Rhodochrosite Mechanisms of Precipitation

Supersaturated solutions (Ω 2–5) containing Mn^{2+}, HCO^-, and CO_3^{2-} were found to remain metastable for >24 h (Table 1). Table 1 shows that the assumption of systems in equilibrium is not satisfactory and kinetic aspects become relevant. Addition of rhodochrosite seeds, in the absence of DOC, induced precipitation that continued until the solution reached equilibrium with respect to rhodochrosite precipitation ($\Omega = 1$, Table 1). We consider that crystal growth is the dominant mechanism for rhodochrosite precipitation under these conditions. In contrast, $MnCO_3$ precipitation occurred in the absence of crystal seeds in solutions with Ω values >10. After filtering the supersaturated solutions, scanning electron microscope observation of the 0.1-μm filters showed the presence of <2-μm crystals. The mineral phase was confirmed by X-ray difractogram as rhodochrosite. Precipitation in the absence of initial crystals under supersaturated conditions ($\Omega > 10$) indicates that rhodochrosite precipitates by heterogeneous nucleation, forming the initial nuclei by using particles such as dust and bacteria as active nucleation sites.

Table 1. Saturation indices and concentration of HCO_3^- at the initiation of the experiment, and after 1, 24, and 72 h (t = 0, 1, 24, and 72 h, respectively) in the absence of rhodochrosite crystal seeds and in the presence of 2 $m^2 L^{-1}$ of seeds.

Ω (t = 0)	HCO_3^- (t = 0)	HCO_3^- (t = 1 h)	HCO_3^- (t = 24 h)	HCO_3^- (t = 72 h)
		no seeds		
		mmol$_c$ L^{-1}		
2	0.33	0.33	0.33	0.33
3	0.39	0.39	0.39	0.39
4	0.42	0.42	0.42	0.42
5	0.45	0.45	0.45	0.43
10	0.59	0.59	0.40	0.35
25	0.82	0.79	0.43	0.34
		with seeds		
		2 $m^2 L^{-1}$		
2	0.33	0.39	0.33	0.28
3	0.39	0.39	0.39	0.28
4	0.42	0.37	0.35	0.28
5	0.45	0.37	0.35	0.27
10	0.59	0.42	0.31	0.28
25	0.82	0.65	0.40	0.29

Precipitation Rate of Rhodochrosite as Affected by Dissolved Organic Carbon: Heterogeneous Nucleation

We measured the precipitation rate of rhodochrosite in the presence of Suwannee River fulvic acid and leonardite humic acid at 0.035, 5, and 10 kPa P_{CO_2} in solutions with Ω values >40, where heterogeneous nucleation is the active precipitation mechanism. The precipitation rate of rhodochrosite decreased with time and with increasing DOC. Figure 1 shows the rhodochrosite precipitation rate at two concentrations of DOC in a 24-h interval. Fulvic acid reduced the precipitation rate of rhodochrosite (Fig. 1, 2, 3, and 4), while leonardite humic acid did not significantly affect the precipitation (data not shown). These results may be surprising since fulvic and humic acids are considered to contain similar functional groups. However, even though they have a common structural pattern, they have distinct solubility characteristics. Fulvic and humic acids contain a large number of both carboxyl and phenolic hydroxyl groups, with the degree of deprotonation depending on the pH of the solution. At higher pH, the mutual repulsion of the negatively charged sites causes the mol-

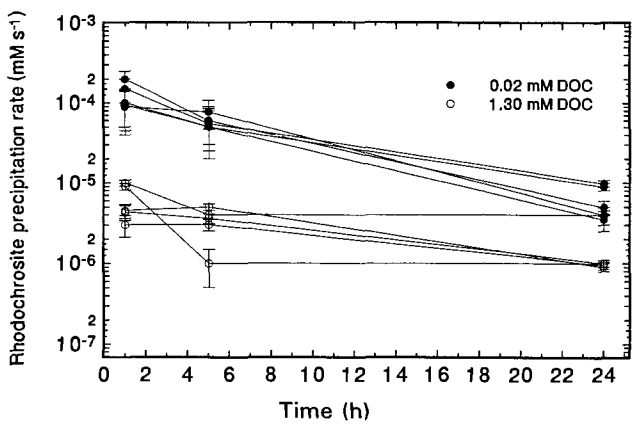

Fig. 1. Rhodocrosite precipitation rate with time at two concentrations of dissolved organic C (DOC).

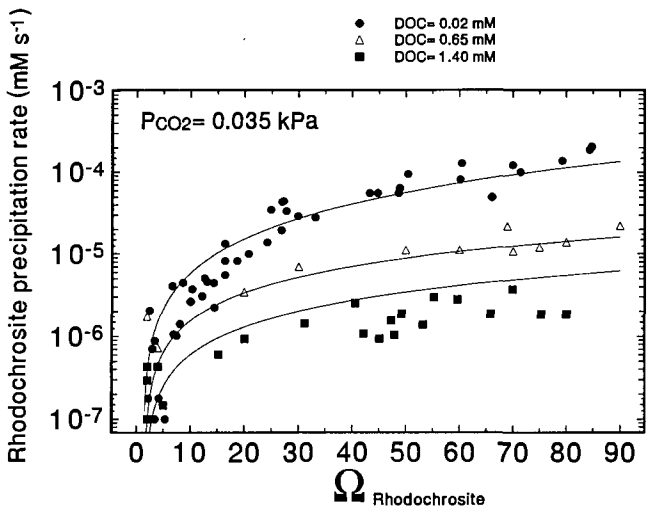

Fig. 2. Rhodochrosite precipitation rate at P_{CO2} = 0.035 kPa as affected by Ω and Suwannee River fulvic acid; dissolved organic C (DOC) = 0.02, 0.65, and 1.40 m*M*. Solid lines represent the precipitation model proposed in the present work.

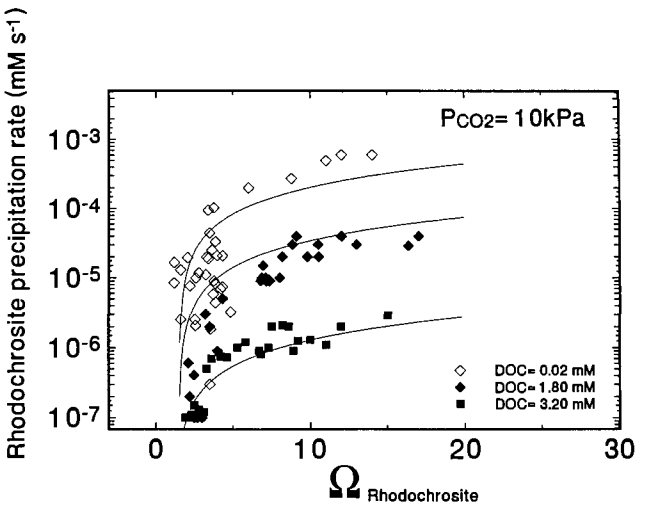

Fig. 4. Rhodochrosite precipitation rate at P_{CO2} = 10 kPa and dissolved organic C (DOC) = 0.02, 1.80, and 3.20 m*M*. Solid lines represent the precipitation model proposed in the present work.

ecule to adopt a stretched configuration. As the pH is lowered and some of the charged sites are neutralized, a reduction in intramolecular repulsion is predicted, and this results in a contraction of the polymer chain. Using fluorescence anisotropy, Engebretson et al. (1996) defined an association index for humic acids. This association index is a quantitative parameter for the estimation of the contraction of the polymer. They found that the association index increases with decreasing pH, consistent with a structural contraction of the humic acid molecule. Comparing the association index of several humic acids, we observed that the leonardite humic acid standard (a large molecule) and a humic acid extracted from Latahco silt loam soil (Argiaquic Xeric Argialbolls) show a much higher association index than the two aquatic humic acids (small molecule) and a soil humic acid standard. This difference is consistent with the relatively smaller molecules' higher number of carboxyl groups, whose mutual repulsion results in a more stretched configuration. Size and flexibility are two of the molecular parameters claimed to govern this behavior. These factors may account for the absence of interaction of humic acids with the charged surface of carbonate crystals, since at least part of the charges are occluded and, thus, possibly neutralized by other ions within the humic acid.

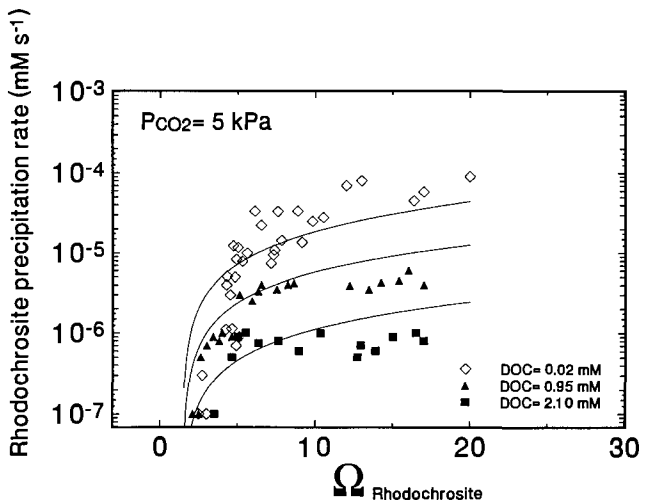

Fig. 3. Rhodochrosite precipitation rate at P_{CO2} = 5 kPa and dissolved organic C = 0.02, 0.95, and 2.10 m*M*. Solid lines represent the precipitation model proposed in the present work.

The decreased influence of humic acid on the precipitation rate of carbonate minerals agrees with data in the literature where Pachappa soil extract was found to have only 1/3 of the inhibitory effect on the calcite precipitation rate compared with that of the Suwannee River fulvic acid reference. The DOC derived from Pachappa soil extract is 26.5% fulvic acids and 70% humic acids (Lebron and Suarez, 1996).

Table 2 presents the initial concentrations of HCO_3^-, Mn^{2+}, and pH and the activities of the complexes $MnHCO_3^+$ and $MnFulv^+$ for the three P_{CO2} and three concentrations of DOC. From Table 2 we observe that the complexation $Mn–Fulv^+$ increases when P_{CO2} and DOC concentration increases.

Crystal Growth

The rhodochrosite precipitation rate decreased with increased DOC adsorption for the three concentrations of P_{CO2} (Fig. 5). The reduction in precipitation rate of calcite has been observed by other authors (Inskeep and Bloom, 1986, Inskeep and Silvertooth, 1988; Lebron and Suarez, 1996) and has been interpreted as the blocking of active sites on the mineral surface by the organic functional groups. We observed that when the P_{CO2} increased, higher coverage of DOC was necessary to produce an equivalent reduction in the rhodochrosite precipitation rate (Fig. 5). The requirement of greater DOC concentrations to inhibit precipitation at greater P_{CO2} may be due to an increase in the negative surface charge of the rhodochrosite surface coupled with a possible lower reactivity of DOC under the conditions of higher P_{CO2}. Notice from Table 2 that even though $Mn–Fulv^+$ complexation is important when DOC increases,

Table 2. Initial concentrations (t = 0) for HCO_3^-, Mn^{2+}, dissolved organic C (DOC) and calculated final DOC and Mn complexes for three partial pressures of CO_2 using GEOCHEM-PC.

P_{CO2}	DOC (t = 0)	DOC_{free}	pH	HCO_3^- (t = 0)	Mn^{2+} (t = 0)	Mn–HCO_3^+	Mn–Fulv$^+$
kPa	mM			mmol$_c$ L^{-1}		Activities	
0.035	0.02	0.02	8.23	1.29×10^{-3}	1.15×10^{-3}	2.15×10^{-5}	2.95×10^{-6}
0.035	0.65	0.56	8.26	1.28×10^{-3}	1.18×10^{-3}	1.82×10^{-5}	8.07×10^{-5}
0.035	1.40	1.23	8.30	1.23×10^{-3}	1.15×10^{-3}	1.67×10^{-5}	1.68×10^{-4}
5	0.02	0.01	6.41	2.26×10^{-3}	2.19×10^{-3}	1.52×10^{-4}	7.46×10^{-6}
5	0.95	0.61	6.42	2.26×10^{-3}	2.20×10^{-3}	1.32×10^{-4}	3.18×10^{-4}
5	2.10	1.45	6.45	2.32×10^{-3}	2.22×10^{-3}	1.08×10^{-4}	6.05×10^{-4}
10	0.02	0.01	6.29	3.81×10^{-3}	3.75×10^{-3}	3.54×10^{-4}	8.89×10^{-6}
10	1.80	1.03	6.30	3.63×10^{-3}	3.50×10^{-3}	2.59×10^{-4}	7.10×10^{-4}
10	3.20	2.00	6.32	3.68×10^{-3}	3.51×10^{-3}	2.21×10^{-4}	1.11×10^{-3}

when the P_{CO2} increased we still required higher DOC concentrations to cause a similar reduction in the precipitation rate. A detailed discussion of this P_{CO2} effect presented in Lebron and Suarez (1998) for calcite is also applicable here.

We calculated Langmuir adsorption isotherms for Suwannee River fulvic acid on the surface of rhodochrosite for the three P_{CO2} levels using the program ISOTHERM (Kinniburgh, 1986). The calculated isotherm lines and the experimental data are shown in Fig. 6. The isotherm is expressed as

$$C_{ads} = K \times M \times \text{DOC}/(1 + K \times \text{DOC}) \quad [1]$$

where M is the maximum adsorption and K is the affinity constant. Table 3 shows the coefficients of the calculated isotherms for the three P_{CO2} levels studied. Also shown in Table 3 is the calculated DOC concentration in solution necessary to completely inhibit the $MnCO_3$ precipitation (C_{inh}). This value was calculated from the isotherm data as surface DOC coverage necessary to inhibit precipitation. The results in Table 3 show a lower affinity of the DOC for rhodochrosite than for calcite at atmospheric P_{CO2}. This observation is based on comparison of the affinity constant value for calcite, 20 mmol^{-1} L (Lebron and Suarez, 1998), with the K value for rhodochrosite, 17.6 mmol^{-1} L. Only 0.05 mM DOC is necessary to inhibit calcite crystal growth at atmospheric P_{CO2}, while 0.15 mM DOC is needed to inhibit rhodochrosite crystal growth. Similar concentrations of DOC were found to inhibit crystal growth for the calcite and rhodochrosite system at P_{CO2} 5 and 10 kPa.

Precipitation Rate of Rhodochrosite as Affected by P_{CO2}

The precipitation rate of rhodochrosite increased when the P_{CO2} increased from 0.035 kPa to 10 kPa in the range of Ω 1 to 35 (Fig. 7). Charlet et al. (1990) used a fast acid–base titration technique and found that rhodochrosite has a higher density of negative charge when the P_{CO2} increases, which is due to changes in surface speciation in systems with a pH > pH of zero point of charge (pH_{ZPC}). The implications for our system are that, for the same Ω value, the number of active sites on the surface of rhodochrosite is higher with increasing P_{CO2}, since the pH in our experiments was always above the pH_{ZPC}.

Plummer et al. (1978) proposed that the precipitation mechanism for calcite was the reaction between bulk solution $CaHCO_3^+$ and negatively charged surface sites. By analogy, we calculated the activity of different species in solution for designated samples using the speciation program GEOCHEM-PC (Parker et al., 1994). The samples have the same supersaturation but different P_{CO2} levels. For Ω = 3.5, the $MnHCO_3^+$ activity was 2.8×10^{-6} for P_{CO2} = 0.035 kPa and 3.3×10^{-5} for P_{CO2} = 10 kPa. This agrees with the observation of an increase in the precipitation rate of rhodochrosite when the P_{CO2}

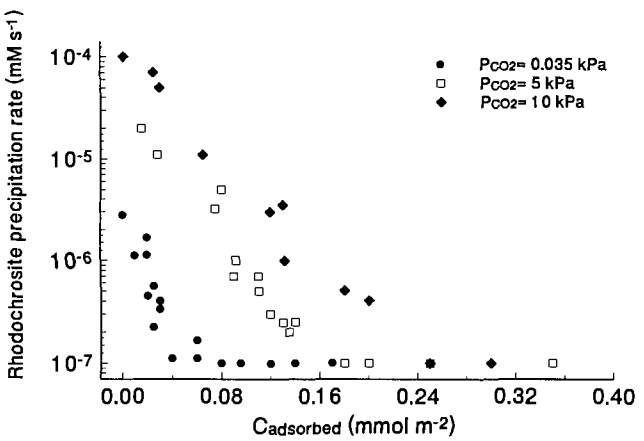

Fig. 5. Rhodochrosite precipitation rate by crystal growth as a function of organic C adsorbed on the surface of the crystals at P_{CO2} 0.035, 5, and 10 kPa.

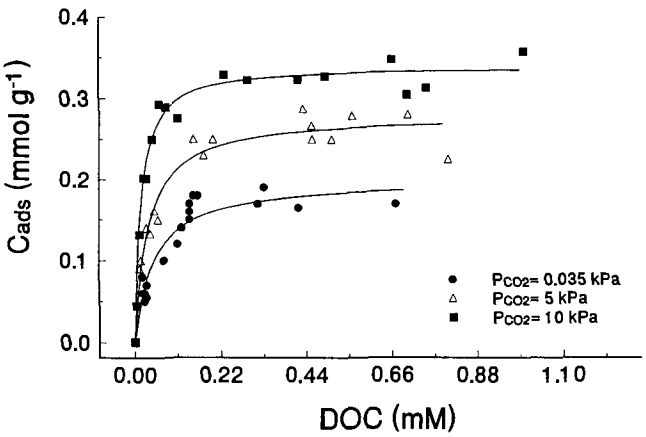

Fig. 6. Langmuir adsorption isotherms for dissolved organic C (DOC) adsorbed on rhodochrosite at P_{CO2} 0.035, 5, and 10 kPa. The equation used is $C_{ads} = M\,K\,\text{DOC}/(1 + K\,\text{DOC})$, where M is the maximum adsorption and K is the affinity constant.

Table 3. Langmuir isotherm parameters for three P_{CO2}, amount of dissolved organic C (DOC) necessary to inhibit crystal growth (C_{inh}), and DOC in equilibrium with C_{inh} (DOC_{eq}).

P_{CO2}	K	M	C_{inh}	DOC_{eq}
kPa	$mmol^{-1}$ L	mmol m^2		m*M*
0.035	17.6	0.11	0.08	0.15
5	23.7	0.23	0.18	0.15
10	25.2	0.33	0.25	0.12

increases. Surface complex-formation constants correlate with the formation constants of the corresponding complexes in solution (Schindler et al., 1976; Kummert and Stumm, 1980; Sigg and Stumm, 1981; Schindler and Stumm, 1987). Consequently, we can assume that the external surface composition of the crystal is similar to that in the bulk solution (van Capellen et al., 1993). The increase in $MnHCO_3^+$ activity together with the increase in the surface negative charge likely explains the measured increase in the rhodochrosite precipitation rates with increasing P_{CO2} at constant Ω (Fig. 7). This increase in the precipitation rates at higher P_{CO2} values has implications for the chemistry of the soil and in the transport of pH-dependent elements. The implications are related with the underestimation of the precipitation and consequent inaccuracy in transport modeling attempts.

Precipitation Rate Equation

The precipitation of rhodochrosite in the presence of fulvic substances can be expressed by the following equation:

$$R_T = R_{CG} + R_{HN} \quad [2]$$

where R_T is the total precipitation rate in m*M* s^{-1}, R_{CG} is the precipitation rate due to crystal growth, and R_{HN} is the precipitation rate due to heterogeneous nucleation. Sternbeck (1997) studied the precipitation of rhodochrosite by crystal growth in the absence of DOC at P_{CO2} of 0.031, 0.15, and 1 kPa and calculated the constants for the following expression:

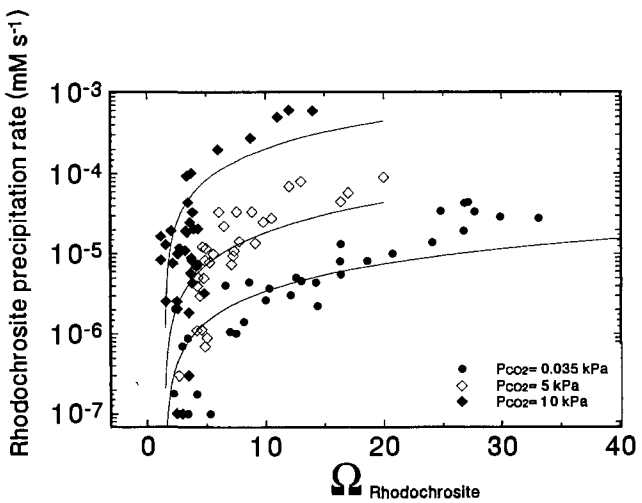

Fig. 7. Rhodochrosite precipitation rate as a function of rhodochrosite supersaturation for three P_{CO2} in the absence of dissolved organic C. Solid lines represent the precipitation model proposed in the present work.

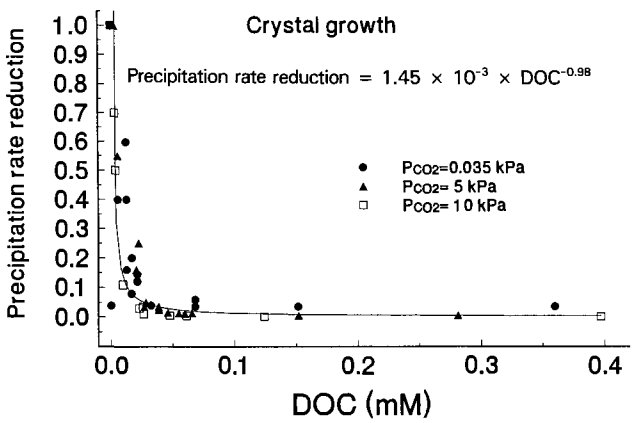

Fig. 8. Reduction in the rate of rhodochrosite precipitation by crystal growth as a function of dissolved organic C (DOC) at three different P_{CO2}. Calculations were made by dividing the precipitation rate of rhodochrosite in the absence of DOC by the precipitation rate of rhodochrosite at different DOC concentrations.

$$R_{CG} = k_{CG} \times (\Omega - 1)^n \quad [3]$$

where k_{CG} is 4.97×10^{-8} and 5.47×10^{-8} for P_{CO2} = 0.031, 1. We extrapolated the value of 1.54×10^{-5} m*M* s^{-1} at 10 kPa from the data given by Sternbeck (1997). In our experiments precipitation by crystal growth decreased in the presence of DOC and increased with increasing P_{CO2}. The crystal growth rate equation is expressed as follows:

$$R_{CG} = k_{CG} \times (\Omega - 1)^n f(\mathrm{DOC},P_{CO2}) \quad [4]$$

The factor f(DOC, P_{CO2}) was calculated by representing the precipitation rate reduction of the rhodochrosite as the precipitation rate in the absence of DOC divided by the precipitation rate measured in the presence of different DOC concentrations. The calculated precipitation rate reduction at the three levels of P_{CO2} studied are shown in Fig. 8. In the absence of DOC we found no significant differences between the reduction in precipitation of rhodochrosite at different P_{CO2} for the range of P_{CO2} studied. The following equation was developed to represent the precipitation reduction factor for DOC

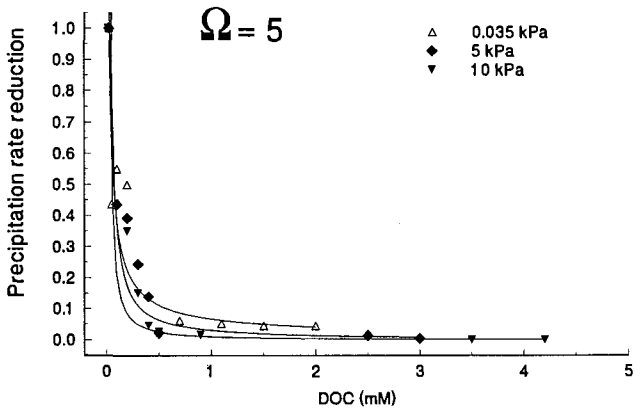

Fig. 9. Reduction in the rate of rhodochrosite precipitation by heterogeneous nucleation as a function of dissolved organic C (DOC) at three different P_{CO2}. Calculations were made by dividing the precipitation rate of rhodochrosite in the absence of DOC by the precipitation rate of rhodochrosite at different DOC concentrations.

at all levels of P_{CO2} (R^2 = 0.63):

$$f(DOC) = 1.45 \times 10^{-3} \times DOC^{-0.98} \quad [5]$$

The precipitation rate term for heterogeneous nucleation is expressed as:

$$R_{HN} = k_{HN}(\Omega - 1.5)f(DOC,P_{CO2}) \quad [6]$$

where k_{HN} is the precipitation rate constant, and f(DOC, P_{CO2}) is a factor that includes the effect of the DOC and the P_{CO2} in the rhodochrosite precipitation rate. For our experimental results the rate reduction factor is described by the following expression:

$$f(DOC,P_{CO2}) = 10^{a+b\,DOC+cP_{CO2}} \quad [7]$$

where a, b, and c are constants. Similar to the crystal growth term, the constants in Eq. [7] were calculated from a separate experiment. Precipitation rate reduction values were calculated by dividing the rhodochrosite precipitation rate in the absence of DOC by the precipitation rate in the presence of different DOC concentrations. Comparable calculations were made for reduction rates at 0.035, 5, and 10 kPa (Fig. 9). The values of the constants for Eq. [6] are: $k_{HN} = 1.05 \pm 6.2 \times 10^{-2}$ mMs^{-1}, $a = -6.39 \pm 8.6 \times 10^{-2}$ (dimensionless), $b = -0.55 \pm 3.4 \times 10^{-2}$ mM^{-1}, and $c = 1.05 \pm 6.2 \times 10^{-2}$ kPa^{-1}. The R^2 for the model was 0.661 and all parameters were highly significant.

The representation of Eq. [2] is shown in solid lines in Fig. 2 through 4, which indicate agreement between the predicted and experimental results. For $P_{CO2} < 10$ kPa the model provided good prediction for all but the date at high DOC and high Ω. Even though the model can be improved by further studies, the simplicity of the mathematical expression justifies this initial attempt. More studies are needed to evaluate other important factors affecting rhodochrosite precipitation, especially interaction with calcite.

CONCLUSIONS

Prediction of Mn^{2+} concentration in reduced alkaline soils will depend on the kinetics of Mn oxidation and rhodochrosite precipitation; the assumption of equilibrium is not satisfactory in many natural systems. Crystal growth and heterogeneous nucleation have been identified as the two precipitation mechanisms for rhodochrosite. However, the presence of 0.15 mM of DOC was enough to inactivate the crystal growth mechanism, which resulted in metastable solutions supersaturated with respect to rhodochrosite (Ω 2–5). The DOC concentration of 0.15 mM is in the range of concentrations typically observed in soil solutions. The precipitation of rhodochrosite shows many similarities with the precipitation of calcite. However, at atmospheric P_{CO2} precipitation of rhodochrosite by crystal growth has been shown to be a more relevant mechanism than is the case for calcite. This is due to a lower affinity of DOC for rhodochrosite as compared with calcite at atmospheric CO_2. The precipitation rate of rhodochrosite increased when the P_{CO2} increased. This increment in the precipitation rate can be explained in terms of surface speciation with an increase in the negative charge on the rhodochrosite surface when the P_{CO2} increases. The addition of fulvic acid reduced the precipitation rate of rhodochrosite one order of magnitude when the DOC increased from 0.02 to 1.3 mM, but the precipitation rate was not affected when leonardite was used. The reason for the lack of inhibitory properties for leonardite may be related to the spatial configuration of its humic acids. A model is presented to predict the kinetics of precipitation of rhodochrosite at different supersaturation levels and different P_{CO2} and DOC concentrations.

REFERENCES

Balistrieri, L.S., and J.W. Murray. 1982. The surface chemistry of δMNO_2 in major ion seawater. Geochim. Cosmochim. Acta 46:1041–1052.

Boyle, E.A. 1983. Manganese carbonate overgrowths in foraminifera tests. Geochim. Cosmochim. Acta 47:1815–1819.

Charlet, L., P. Wersin, and W. Stumm. 1990. Surface charge of $MnCO_3$ and $FeCO_3$. Geochim. Cosmochi. Acta 54:2329–2336.

Crerar, D.A., R.K. Cormick, and H.L. Barnes. 1980. Geochemistry of Manganese: An overview. p. 293–334. *In* I.M. Varentsov and G.Y. Grasselly (ed.) Geology and Geochemistry of manganese. Vol. 1. Proc. 2nd Int. Symposium on Geology and Geochemistry of Manganese. Sidney, Australia. 17–24 August 1980. E. Schweizerbart'sche Verlagsbuchhdlg. Stuttgart, Germany.

Dove, P.M., and M.F. Hochella, Jr. 1993. Calcite precipitation mechanisms and inhibition by orthophosphate: In situ observations by scanning force microscopy. Geochim. Cosmochim. Acta 57:705–714.

Engebretson, R.R., T. Amos, and R. Von Wandruszka. 1996. Quantitative approach to humic acid associations. Environ. Sci. Technol. 30:990–997.

Friedl, G., B. Wehrli, and A. Manceau. 1997. Solid phases in the cycling of manganese in eutrophic lakes: New insights from EXAFS spectroscopy. Geochim. Cosmochim. Acta 61:275–290.

Gratz, A.J., and P.E. Hillner. 1993. Poisoning of calcite growth viewed in the atomic force microscope (AFM). J. Crys. Growth 129: 789–793.

Inskeep, W.P., and P.R. Bloom. 1986. Kinetics of calcite precipitation in the presence of water soluble organic ligands. Soil. Sci. Soc. Am. J. 50:1167–1172.

Inskeep, W.P., and J.C. Silvertooth. 1988. Inhibition of hydroxyapatite precipitation in the presence of fulvic, humic, and tannic acids. Soil Sci. Soc. Am. J. 52:941–946.

Jakobsen, R., and D. Postma. 1989. Formation and solid solution behaviour of Ca-rhodochrosites in marine muds of the Baltic deeps. Geochim. Cosmochim. Acta 53:2639–2648.

Katz, J.L., M.R. Reick, R.E. Herzog, and K.I. Parsiegla. 1993. Calcite growth inhibition by iron. Langmuir 9:1423–1430.

Kinniburgh, D.G. 1986. General purpose adsorption isotherms. Environ. Sci. Technol. 20:895–904.

Kitano, Y., and D.W. Hood. 1965. The influence or organic material on the polymorphic crystallization of calcium carbonate. Geochim. Cosmochim. Acta 29:29–41.

Kummert, R., and W. Stumm. 1980. Surface complexation of organic acids on hydrous γ-Al_2O_3. J. Colloid Interface Sci. 75:373–385.

Lebron, I., and D.L. Suarez. 1996. Calcite nucleation and precipitation kinetics as affected by dissolved organic matter at 25°C and pH >7.5. Geochim. Cosmochim. Acta 60:2765–2776.

Lebron, I., and D.L. Suarez. 1998. Kinetics and mechanisms of precipitation of calcite as affected by P_{CO2} and organic ligands at 25°C. Geochim. Cosmochim. Acta 62:405–416.

Marschner, H. 1988. Mechanisms of manganese acquisition by roots from soils. p. 191–204. *In* R.D. Graham et al. (ed.) Manganese in soils and plants. Kluwer Acad. Publ., Boston.

Norvell, W.A. 1988. Inorganic reactions of manganese in soils. p. 37–58. In R.D. Graham et al. (ed.) Manganese in soils and plants. Kluwer Acad. Publ., Boston.

Okita, P.M. 1992. Manganese carbonate mineralization in the Molango District, Mexico. Econ. Geol. 87:1345–1366.

Paquette, J., H. Vali, and A. Mucci. 1996. TEM study Pt-C replicas of calcite overgrowths precipitated from electrolyte solutions. Geocim. Cosmochim. Acta 60:4689–4699.

Parker, D.R., W.A. Norvell, and R.L. Chaney. 1994. GEOCHEM-PC: A chemical speciation program for IBM and compatible personal computers. p. 253–270. *In* R.H. Loeppert et al. (ed.) Soil chemical equilibrium and reaction models. SSSA Spec. Publ. 42, ASA and SSSA, Madison, WI.

Pederson, T.F., and N.B. Price. 1982. The geochemistry of manganese carbonate in Panama Basin sediments. Geochim. Cosmochim. Acta 46:59–68.

Plummer, L.N., T.M.L. Wigley, and D.L. Parkhurst. 1978. The kinetics of calcite dissolution in CO_2: Water systems at 5° to 60° C and 0.0 to 1.0 atm CO_2. Am. J. Sci. 278:179–216.

Reddy, M.M. 1977. Crystallization of calcium carbonate in the presence of trace concentrations of phosphorous containing anions I. Inhibition by phosphate and glycerophosphate ions at pH 8.8 and 25°C. J. Crys. Growth 41:287–295.

Reddy, M.M., and K.K. Wang. 1980. Crystallization of calcium carbonate in the presence of metal ions I. Inhibition by magnesium ion at pH 8.8 and 25°C. J. Crys. Growth 50:470–480.

Reynolds, R.C., Jr. 1978. Polyphenol inhibition of calcite precipitation in Lake Powell. Limnol. Oceanogr. 23:585–597.

Schindler, P.W., and W. Stumm. 1987. The surface chemistry of oxides, hydroxides, and oxide minerals. p. 83–110. *In* W. Stumm (ed.) Aquatic surface chemistry. J. Wiley & Sons, New York.

Schindler, P.W., B. Furst, R. Dick, and P.U. Wolf. 1976. Ligand properties of surface silanol groups. I. Surface complex formation with Fe^{3+}, Cu^{2+}, Cd^{2+} and Pb^{2+}. J. Colloid Interface Sci. 55:469–475.

Sigg, L., and W. Stumm. 1981. The interaction of anions and weak acids with the hydrous goethite (α-FeOOH) surface. Colloids Surf. 2:101–117.

Sposito, G., K.M. Holtzclaw, and J. Baham. 1976. Analytical properties of the soluble, metal-complexing fractions in sludge–soil mixtures. II. Comparative structural chemistry of fulvic acid. Soil Sci. Soc. Am. J. 40:691–697.

Sternbeck, J. 1997. Kinetics of rhodochrosite crystal growth at 25°C: The role of surface speciation. Geochim Cosmochim. Acta 61: 785–793.

Suarez, D.L., J.D. Wood, and I. Ibrahim. 1992. Reevaluation of calcite supersaturation in soils. Soil Sci. Soc. Am. J. 56:1776–1784.

van Capellen, P., L. Charlet, W. Stumm, and P. Wersin. 1993. A surface complexation model of the carbonate mineral–aqueous solution interface. Geochim. Cosmochim. Acta 57:3505–3518.

Wartel, M., M. Skiker, Y. Auger, and A. Boughriet. 1990. Interaction of manganese (II) with carbonates in seawater: Assessment of the solubility product of $MnCO_3$ and Mn distribution coeficient between the liquid phase and $CaCO_3$ particles. Mar. Chem. 29:99–117.

Wolfram, O., and R.E. Krupp. 1996. Hydrothermal solubility of rhodochrosite, Mn(II) speciation, and equilibrium constants. Geochim. Cosmochim. Acta 60:3983–3994.